Topological electronic structure and Rashba effect in Bi thin layers: theoretical predictions and experiments

K. Hricovini, M C Richter, O. Heckmann, L Nicolaï, J.-M Mariot, J. Minár

Topical Review

Topological electronic structure and Rashba effect in Bi thin layers: theoretical predictions and experiments

K. Hricovini[1,2]‡, M. C. Richter[1,2], O. Heckmann[1,2], L. Nicolaï[3], J.-M. Mariot[4,5], and J. Minár[3]

[1] Laboratoire de Physique des Matériaux et des Surfaces, Université de Cergy-Pontoise, 5 mail Gay-Lussac, 95031 Cergy-Pontoise, France
[2] DRF, IRAMIS, SPEC – CNRS/UMR 3680, Bât. 772, L'Orme des Merisiers, CEA Saclay, 91191 Gif-sur-Yvette Cedex, France
[3] New Technologies-Research Center, University of West Bohemia, Univerzitní 8, 306 14 Pilsen, Czech Republic
[4] Sorbonne Université, CNRS (UMR 7614), Laboratoire de Chimie Physique–Matière et Rayonnement, 4 place Jussieu, 75252 Paris Cedex 05, France
[5] Synchrotron SOLEIL, L'Orme des Merisiers, Saint-Aubin, BP 48, 91192 Gif-sur-Yvette, France

E-mail: karol.hricovini@u-cergy.fr

Abstract. The goal of the present review is to cross-compare theoretical predictions with selected experimental results of spin- and angle-resolved photoelectron spectroscopy on bismuth thin films exhibiting topological properties and a strong Rashba effect. Despite the bulk Bi crystal is topologically trivial, a single free-standing Bi(1 1 1) bilayer has been predicted by calculations to be a topological insulator. This triggered a large series of studies of ultrathin Bi(1 1 1) films grown on various substrates. Using selected examples we review theoretical predictions of atomic and electronic structure of Bi thin films exhibiting topological properties due to interaction with a substrate. We survey as well experimental signatures of topological surface states, as obtained namely by angle-resolved photoelectron spectroscopy.

PACS numbers: 79.60.-i, 79.60.Dp, 71.70.Ej, 71.20.-b

Keywords: bismuth, topological insulators, Rashba effect, angle-resolved photoemission, spin-resolved photoemission, electronic structure calculations

Submitted to: *Institute of Physics Publishing*
J. Phys.: Condens. Matter

‡ Corresponding author.

1. Introduction

Bismuth, a group V element, has been extensively studied because of its extreme physical properties: among the metals, it has as the highest magnetic susceptibility, a very high resistivity, one the lowest heat conductivity and the highest Hall coefficient [1]. Being the heaviest non-radioactive element, Bi exhibits a strong spin-orbit coupling (SOC). It is as well the parent of several topological insulators (TIs). Thus Bi is a good candidate to produce novel topological systems. Another important aspect of Bi is the clear manifestation of quantum size effects because its Fermi wavelength is one order of magnitude larger than that in most metals (see, e.g. [2]).

Two-dimensional (2D) TIs, called also quantum spin Hall insulators, have attracted a lot of attention due to many exotic properties that originate in strong SOC. In the bulk, TIs hold charge excitation gaps, whereas the surface is characterized by metallic states in one dimensional (1D) edges (for 2D TIs) or 2D surfaces (for 3D TIs). In these metallic channels, opposite flowing charge currents are locked to the opposite spins. These states are robust against backscattering by nonmagnetic impurities and thus suited for future spintronic devices and quantum computation (see, e.g. [3, 4]).

Strong SOC is also at the heart of the Rashba effect, an important physical phenomenon for developing next-generation spintronic devices, since it enables the manipulation of spin-polarized electrons without using a magnetic field [5, 6]. Rashba interaction becomes larger in materials with heavy atoms due to the larger atomic SOC. This is why Bi has provided an excellent platform for investigating the Rashba effect and the characteristics of the spin structure.

Bulk Bi crystal is topologically trivial, but a single, free-standing, Bi(1 1 1) bilayer (BL) has been theoretically predicted to be a 2D TI [7]. The lattice distortion of the Bi(1 1 1) film on a suitable substrate, a parameter that can be controlled in thin films, allows to tune the Rashba effect and plays an essential role for the band inversion which is a key ingredient in topologically non-trivial materials.

Angle-resolved photoelectron spectroscopy (ARPES) and its spin-resolved version (SARPES) are particularly well suited to probe the electronic structure and investigate bulk/surface states in solids [8–10]. PES relies on the photoelectric effect, i.e. the electron emission consecutive to the shining of a material by X-UV radiation. The measurement of the kinetic energy (E_{kin}) distribution of the photoelectrons induced by a monochromatic X-UV light of energy $h\nu$ allows to access to the electron binding energy (E_b) distribution in the solid from the energy conservation law $h\nu = E_b + E_{kin} + \phi$, where ϕ is the work function of the sample. Moreover, by measuring the angular dependence of the photoemitted intensity, one can, through the conservation of the photoelectron momentum along the surface direction, map band dispersions and Fermi surfaces. Further information on the spin polarization (SP) of the electronic states is provided through the detection of the spin of the photoemitted electrons [11].

After recalling some of the major structural and electronic properties of bulk Bi (section 2), we put emphasis on Bi thin films (section 3). The thin film growth is first

discussed (section 3.1); the electronic surface states, the Rashba effect (section 3.2) and the spin-related issues (section 3.3) are then addressed; these sections are followed by considerations on the topological aspects of Bi thin layers *per se* or deposited on TIs (sections 3.4 and 3.5, respectively) and on edge states (section 3.6); finally a short discussion on the emerging bismuthene physics (section 3.7) and on possible future prospects (section 3.8) is made, before a summary (section 4) is given.

2. Electronic structure of bulk bismuth

In this section we recall briefly the main physical properties of bulk Bi and the first photoemission experiments on Bi monocrystals, necessary to understand the behaviour of thin films.

2.1. Basic properties

Bismuth bulk and surfaces properties have recently been exhaustively reviewed [2]. Here we summarize only the main features. Bismuth is a peculiar example of system exhibiting marked differences between surface and bulk properties. All its crystallographic surfaces are much better metals than the bulk due to the existence of electronic surface states.

Bismuth monocrystal has rhombohedral symmetry which is typical for the group V semimetals [space group $R\bar{3}m$ (No. 166; Strukturbericht A7, α-As structure)]. In bulk Bi, each atom has three equidistant nearest neighbours, other three equidistant next-nearest neighbours being placed at slightly longer distance. This results in buckled BLs of atoms perpendicular to the [1 1 1] direction in which each atom is covalently bonded to its three nearest neighbours [figure 1(a)]. The next-nearest neighbours are in the adjacent BLs and the bonding within each BL is much stronger than the van der Waals inter-BL bonding, explaining that cleavage along {1 1 1} is easy [12] [figure 1(b)].

The electronic structure of rhombohedral Bi and of the very similar simple cubic structure deserve to be confronted. In the latter case, the two atoms of the rhombohedral unit cell become equivalent: the unit cell contains only one atom with five valence electrons, i.e. an odd number. Therefore, from an electron counting argument, the cubic structure is expected to have a partially filled valence band and to be metallic. On the contrary, there are ten valence electrons for the rhombohedral unit cell, which leads to an insulating behaviour, and to a semimetallic behaviour in presence of a faint band overlap. This suggests that, as these two structures are very similar, structural changes at surfaces are expected to have an important impact on the electronic structure [2].

Bismuth is behaving as a semimetal and many of its unique properties are closely related to its very special electronic structure. The bulk Brillouin zone of Bi and its projection on the (1 1 1) surface are shown in figure 2. Close to the T and L points the 6*p* bands cross the Fermi level, creating hole pockets at the T points and electron pockets at the L points. These pockets are very shallow; the Fermi level is 27.2 meV for

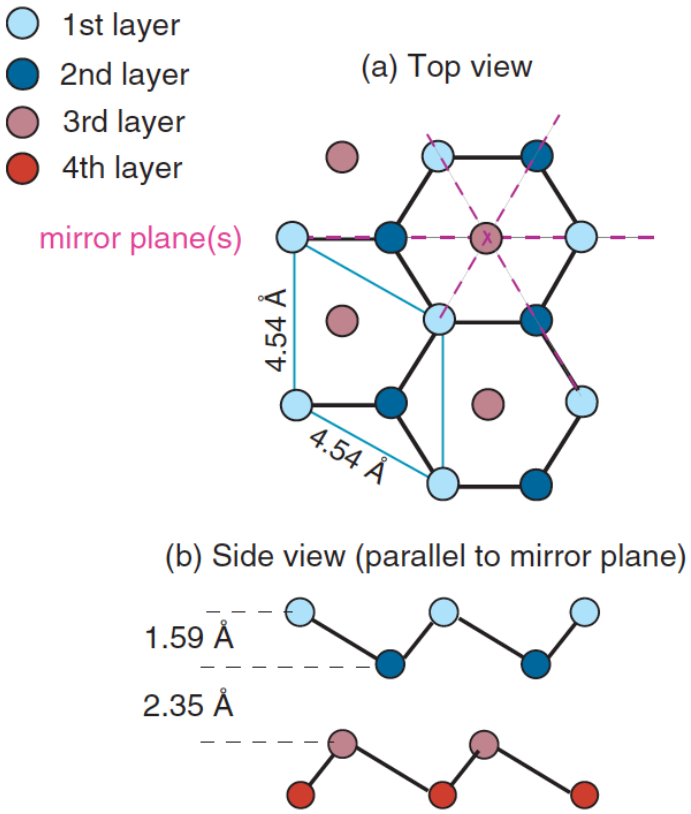

Figure 1. Truncated bulk structure of Bi(1 1 1). The solid lines indicate covalent bonds between the atoms within the bilayers. (a) Top view of the first three atomic layers. Each layer consists of a 2D trigonal lattice. Dashed lines indicate the mirror planes of the structure. (b) Side view (projected onto a mirror plane) of the first four layers. Reprinted figure with permission from [12]. Copyright (2005) by the American Physical Society.

the electrons and 10.8 meV for the holes. The bulk Fermi surface elements projected on the surface Brillouin zone are such that the electron pockets and the hole pockets can be found close to the $\overline{\mathrm{M}}$ and $\overline{\Gamma}$ points, respectively [2].

Interestingly, due to the bulk inversion symmetry, the SOC does not lead to any lifting of the spin degeneracy, on the contrary to the surfaces where this symmetry is broken.

Already about 50 years ago, it has been argued [13] that quantum effects could be present on the (1 1 1) surface. This is mainly due to the small effective mass of the electrons ($m^* \approx 0.003\, m_e$) and to their long wavelength at the Fermi level (~ 12 nm) [2], meaning that defects on the surface are supposed not to play a significant role.

Before taking thin films in a review, it is important to take into account changes in the electronic structure at crystallographic surfaces. We will concentrate here only on the (1 1 1) surface because it is the most important for applications: it is the natural cleavage plane and it is the preferred surface resulting from epitaxial growth. For symmetry reasons, this surface gained even more importance with the advent of TIs.

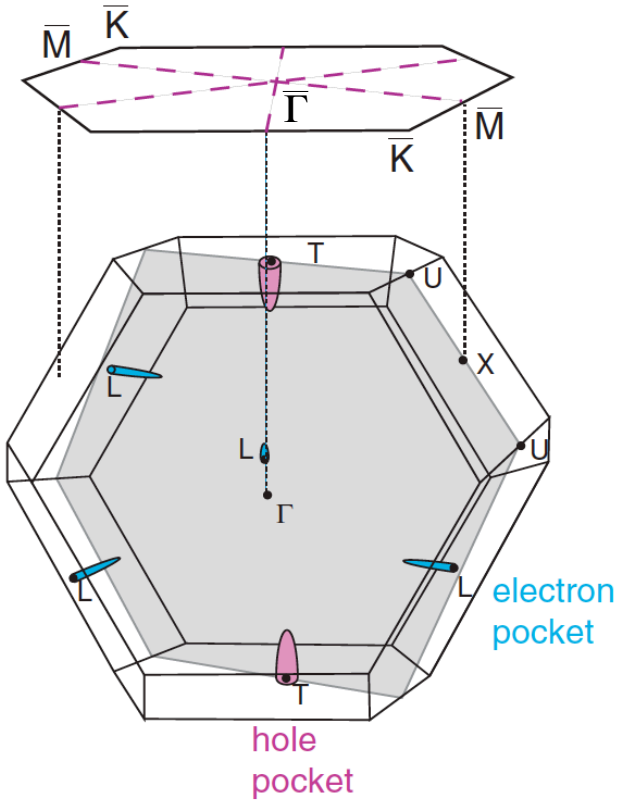

Figure 2. Bismuth bulk Brillouin zone and its projection on the (1 1 1) surface. The elements of the bulk Fermi surface are shown but not to scale. The pink dashed lines indicate the threefold rotational axis and the three mirror lines of the surface Brillouin zone. Adapted from [2], Copyright (2006), with permission from Elsevier.

2.2. Results from photoemission experiments

Pioneering ARPES studies performed on the Bi(1 1 1) face of the bulk crystal were in fair agreement with calculations and shown the presence of surface states in the spin-orbit gaps [14]. Later photoemission measurements, all performed on this surface, refined characterization of the surface states [14–16], revealed a much higher carrier density for the surface and brought the first Fermi surface mapping [17]. It appeared that electronic structure close to the $\overline{\mathrm{K}}$ and $\overline{\Gamma}$ points can be interpreted as modified bulk Bi states. An electron pocket was found at the $\overline{\mathrm{M}}$ point, with a higher effective mass than that expected for the bulk states. Near the $\overline{\Gamma}$ point, the situation is more complex. More detailed studies indicated that the Fermi surface consists of six elongated hole pockets along the $\overline{\Gamma}$–$\overline{\mathrm{M}}$ directions surrounding a ring-shaped electron pocket centred at $\overline{\Gamma}$, all of which have a 2D character. A weak emission feature associated with the bulk hole pocket in the Fermi surface was as well identified [18, 19]. Further characterization briought better understanding of the surface [20] and bulk bands [21]. Two of the four 2D bands lying close to the Fermi level are part of the complex Fermi surface. The threefold rotational symmetry of these bands indicates a weak interaction with the underlying bulk bands.

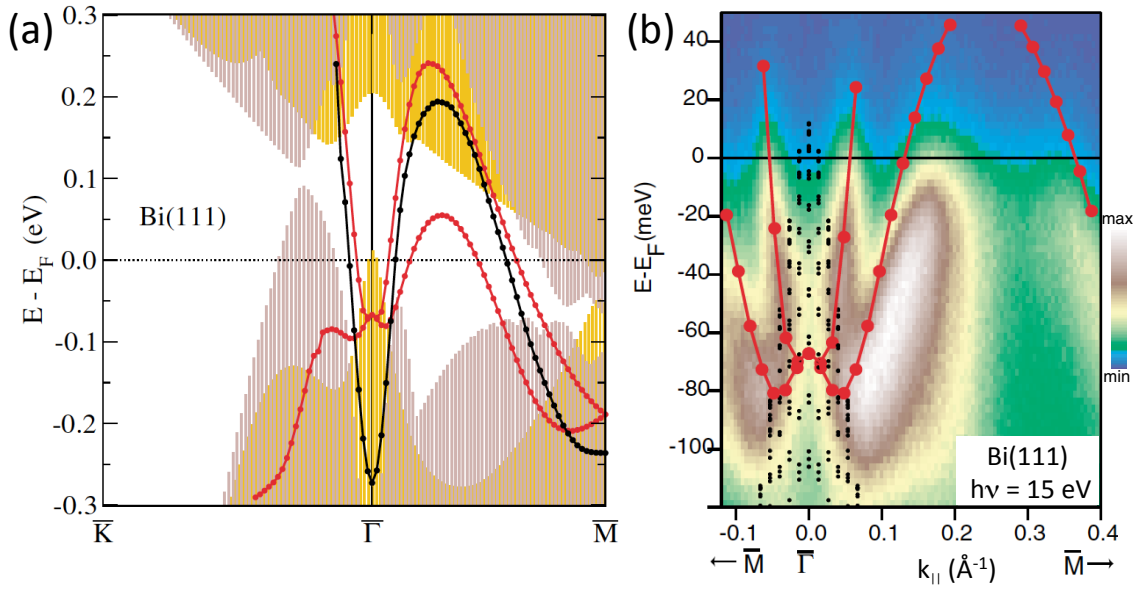

Figure 3. (a) Surface states of Bi(1 1 1) calculated without (black) and with (red) spin-orbit splitting. The shaded areas show the projection of the bulk bands obtained without (violet) and with (yellow) spin-orbit coupling and their superposition (brown). (b) Calculated and measured electronic structure of Bi(1 1 1) along the $\overline{\Gamma}$–$\overline{\mathrm{M}}$ direction. The black dots are the projected bulk band structure calculated using the tight-binding model of Liu and Allen [25]. The red solid circles are the calculated surface state energies; the thin red line is a guide to the eye. The photoemission intensity is linearly scaled from dark blue (minimum) to white (maximum). Reprinted figures with permission from [24]. Copyright (2004) by the American Physical Society.

As Bi is a heavy element, the electronic structure differences between the bulk and the surfaces can be attributed to SOC. The SOC lifts the degeneracy in the bulk electronic structure of solids but this is not the case in solids with inversion symmetry and then the band still contains two possible spin directions. This symmetry is lost at the surface and a $k_{\|}$-dependent splitting of the bands is expected due to the Rashba effect [22, 23]. The first evidence of the influence on the SOC in Bi(1 1 1) was provided by combining experimental data from ARPES with calculations [24] (figure 3).

When the SOC term is included in the calculation, it results in a spin splitting of the surface states in all directions, degeneracy remaining only at the $\overline{\Gamma}$ and $\overline{\mathrm{M}}$ points [red lines in figure 3(a)]. The strong SOC gives as well a qualitative explanation for the fact that the Bi(1 1 1) surface, which can be viewed as the separation of weakly interacting BLs, is metallic despite of the lack of dangling bonds. On the contrary to the situation at the $\overline{\Gamma}$ point where the splitting due to SOC leads to a very steep dispersion of surface states, that at the $\overline{\mathrm{M}}$ point was at the beginning somewhat unclear. Here band degeneracy is expected because $\overline{\mathrm{M}}$ is a high-symmetry point on the surface Brillouin zone boundary. One reason for this difficulty was attributed to the fact that the surface state bands close to the $\overline{\mathrm{M}}$ point are rather surface resonances than genuine surface states.

The ARPES results for Bi(111), shown in figure 3(b), are found to be in good agreement with the calculations for the two split surface states near the $\overline{\Gamma}$ point. The intensity of both surface states strongly decreases in the vicinity of this point, most likely due to the overlap with the projected bulk band structure. The surface states are no longer genuine surface states but surface resonances that penetrate much more deeply into the crystal [24].

SARPES is the most adapted technique for a deeper insight on the lifting of the band degeneracy and the SP. A strong SP of the photocurrent even from bulk continuum states of Bi(1 1 1) has been observed and shown, on the basis of *ab initio* one-step photoemission calculations, to originate from the strong SP of the initial states at the surface and to be the result of the surface sensitivity of SARPES. Final state effects cause deviations of the $\mathbf{k}_{\|}$ dependence of the SP from strictly antisymmetric relative to $\overline{\Gamma}$ [26].

3. Electronic structure of Bi thin films

Today, studies of thin Bi films are still at the centre of a very active research area; so this review can only pretend to give a taste of this rich production. Other recent reviews of theoretical predictions and experimental results obtained by ARPES on Bi surfaces and thin films can be found in references [27–32].

3.1. Growth of thin films

Bismuth on semiconductor surfaces was extensively studied in the 1990s as a typical ordered metal-semiconductor interface. More recently, in the first decade of the 2000s, the interest in thin films was stimulated by the intriguing physical properties of Bi. These studies necessitated good crystalline quality of the films that was mastered namely on the Si(1 1 1)(7×7) substrate [33,34]. Further on, the quality of the layers was improved by mild annealing [35, 36]. In such a way the thickness of stable hexagonal Bi films could be reduced down to 4 BLs [37]. The Si(1 1 1)(7×7) substrate is dominant in the majority of recent reports [33, 35, 38–50].

Other semiconductor surfaces are much less used. Similarly to what happens during the growth on Si(1 1 1), the structure of very thin Bi film is unstable on Ge(1 1 1), its orientation changing from (1 1 0) to (1 1 1) at 6–10 BLs [51]. Here, the strong interaction with the substrate leads to the formation of a hexagonal (1 1 1) film; even at 14 BLs, a lattice constant 2% smaller than that of bulk Bi(1 1 1) is observed.

The particularity of the III–V semiconductors is to have two different terminations of the (1 1 1) surface. From the initial stages of the Bi deposition the growth on the A face (In-terminated InAs) of the InAs(1 1 1) surface is epitaxial, contrary to that on the B face (As-terminated InAs) that proceeds via the formation of islands. ARPES spectra supported by fully relativistic *ab initio* one-step photoemission calculations show that the electronic structure of a 10 BL deposit on the A face is identical to that of bulk

Bi, while more than ~ 30 BLs are needed for the B face [52].

The surface termination controls as well atom mobility-driven structural changes after Bi deposition and upon subsequent annealing. On the A side, a morphology of circular patterns controlled by Bi atoms mobility is observed. On the B side, no particular morphology is observed due to a stronger chemical interaction between Bi and As atoms [53].

Preparation of high quality Bi crystals on other substrates is rather scarce. Quasi layer-by-layer growth mode of Bi nanostructures at low temperature can be realized on highly oriented pyrolytic graphite [54]. Deposition at low temperature, or surfactant-mediated growth, modifies the kinetics of the film growth and enables to get a good film quality even on surfaces of insulators such as α-Al_2O_3(0 0 0 1) [55]. Metallic surfaces can as well be suitable substrates, as this is the case for Ni(1 1 1) [56], Cu(1 1 1) [57] and Au(1 1 1) [58]. In particular, films above 1 BL on Au(1 1 1) preserve the (1 1 0) symmetry up to ~ 60 BL. The structural transition from Bi(1 1 0) to Bi(1 1 1) occurs by heating at 470 K. In general, it is difficult to obtain thick Bi(1 1 0) films and thus the Au(1 1 1) substrate is appropriate for investigation of the peculiar electronic characteristics of Bi(1 1 0) [58].

3.2. Surface states – Rashba effect

The even number of valence electrons makes Bi very close to being an insulator, but the very slight overlap between the conduction and valence bands eventually drives it to a prototype semimetal with a very small number of carriers ($3 \times 10^{17}\,\mathrm{cm}^{-3}$). This leads to an unusually long Fermi wavelength and could open the perspective for the development of devices based on quantum size effects [56, 59]. In this context, it was theoretically proposed that, by making the films thinner, Bi turns from a semimetal into a semiconductor because the related confinement discretizes the perpendicular momentum of the electron and tends to open the gap [60, 61]. In contrast to this scenario, ARPES measurements on ultrathin Bi(1 1 1) films showed surprisingly that the films are highly metallic [38] (figure 4). The long-standing controversy of semimetal to semiconductor transition has finally been resolved. The problem had been controversial because of the subtle fact that the film interior is semiconducting while the surface is always metallic [62].

It is clear that the observed metallic surface states are completely different from the projected bulk. The Fermi surface shown in figures 4(a–c) is formed by a hexagonal electron pocket around the $\overline{\Gamma}$ point and six hole lobes along the $\overline{\Gamma}$–$\overline{\mathrm{M}}$ direction, schematically shown in figure 4(d), very similar identical to the so-called "crown shape" Fermi surface reported on the cleaved surface [18, 19]. These features do not change with the film thickness.

Since the surface states are spin split, the electron and hole doping leads to a switching off of one of the spin channels for surface conductivity, making the doped Bi films potentially interesting for spintronic applications [49]. This can be achieved using

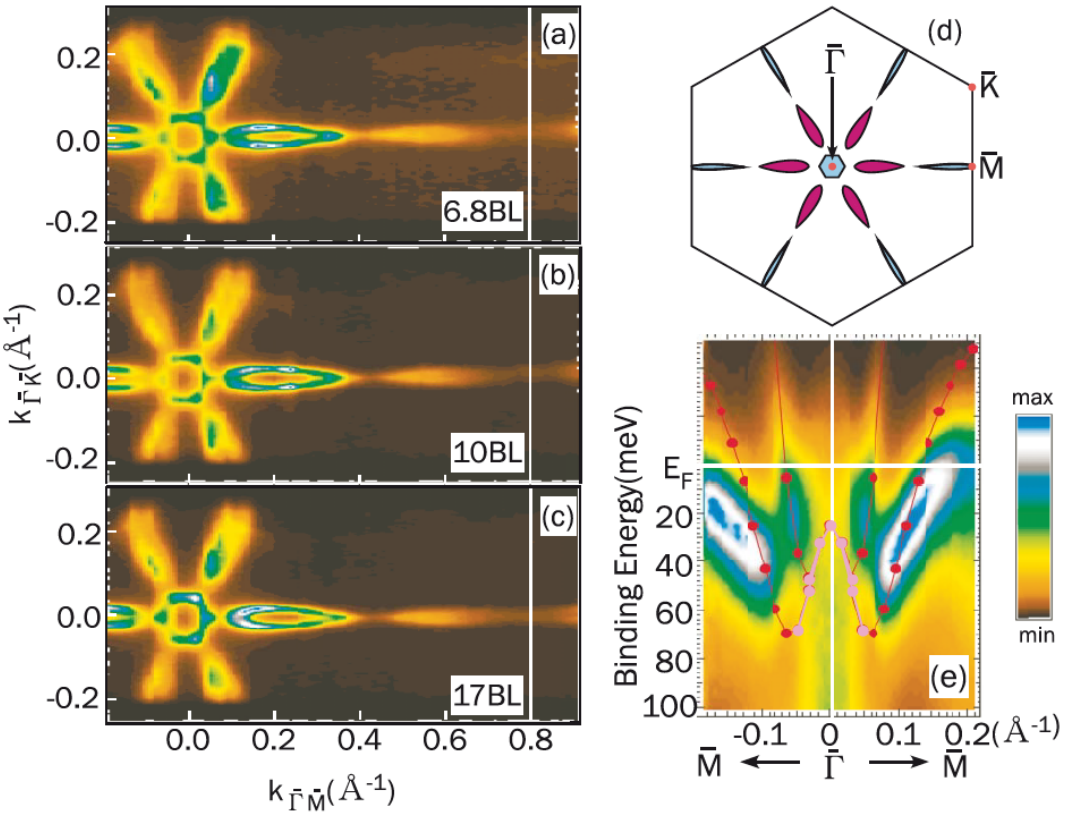

Figure 4. (a–c) The Fermi surface of 6.8, 10 and 17 bilayers (BL) Bi(1 1 1) films, respectively. (d) Schematic drawing of the Fermi surface in the surface Brillouin zone. Electron pockets are coloured in light blue and hole pockets in purple. (e) The band dispersion along the $\overline{\Gamma}$–$\overline{\mathrm{M}}$ direction for the 10 BL film close to the Fermi level. The solid lines through the dots are the results of first-principles calculation with one side of the film terminated with H. The red circles are surface states and the pink ones surface resonances. Reprinted figure with permission from [38]. Copyright (2006) by the American Physical Society.

adsorption of appropriate species. For example upon room temperature adsorption of small amounts of Cs forming a 2D adatom gas, the surface states shift to the higher binding energies by 100–300 meV due to an electronic charge transfer from the Cs adsorbate to the Bi film. As a result, only the electron pockets are left at the Fermi surface. On the contrary, upon adsorption of Sn followed by annealing at 150 °C, Sn atoms dissolve into the Bi film and act as acceptor dopant causing a downward shift by 100 meV, only the hole pockets being left at the Fermi surface.

Additionally, as already suggested by *ab initio* calculations for the bulk crystal [24], the surface states show a large Rashba splitting [63], due to the significant SOC [see figures 3(e) and 4(e)].

A clear momentum-dependent spin splitting and a SP of the surface state bands has been further observed by SARPES. The spin structure was antisymmetric with respect to the $\overline{\Gamma}$ point, as predicted by theory, and the obtained in-plane SP was as high

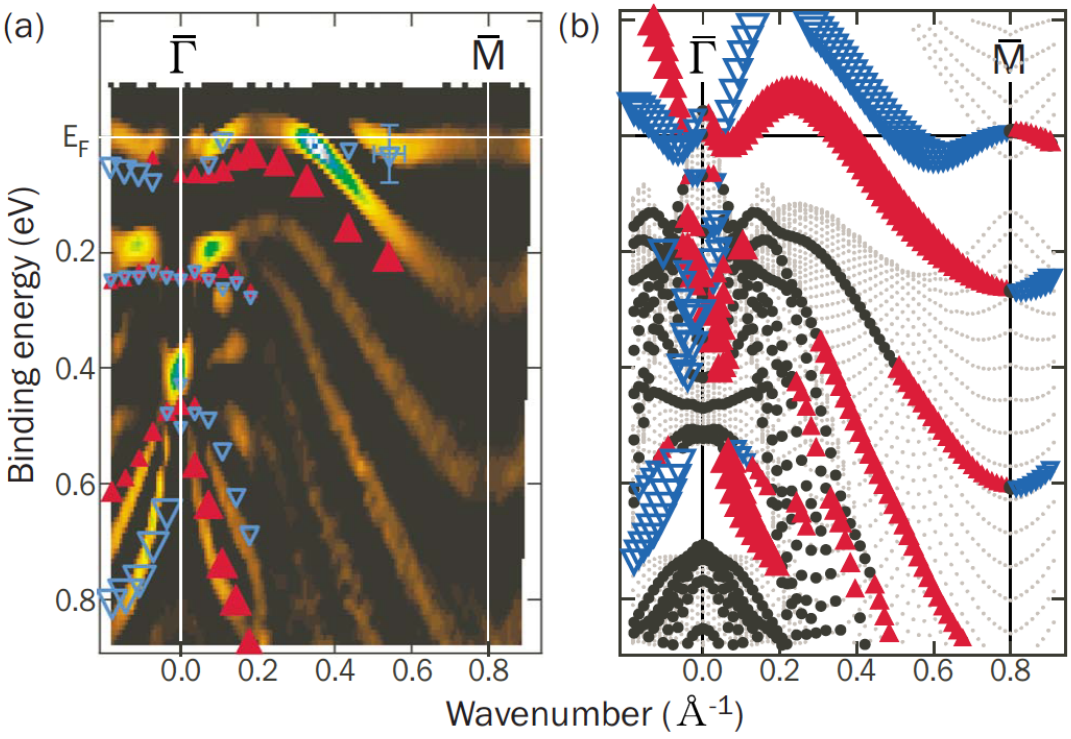

Figure 5. (a) Spin-split band dispersion of a 10 bilayers Bi{1 1 1} film in the $\overline{\Gamma}$–$\overline{\mathrm{M}}$ direction obtained from spin- and angle-resolved photoelectron spectroscopy (triangles) superimposed on non-spin-resolved angle-resolved photoelectron spectroscopy data. (b) The spin-polarized band structure of the *ab initio* calculations for free-standing Bi slabs. The gray dots represent the bulk band projection. In both panels, the spin-up (-down) channels are shown by red (blue) solid triangles, the size of which indicate the magnitude of the spin polarization. Reprinted figure with permission from [40]. Copyright (2007) by the American Physical Society.

as ±0.5 [40]. However, because of the complex band structure of bulk Bi, the surface state bands do not follow, except for small **k**-vectors, the behaviour expected from the Rashba picture in which two concentric circles for the Fermi surface are expected [41].

The Rashba effect plays the dominant role where the surface states are located in the bulk band gap but changes gradually into a parity effect due to quantum confinement where the surface states start to overlap with the bulk band projection. This demonstrates that band splitting due to different symmetry breaking with completely different characteristics can be smoothly joined and suggests an intriguing crossover between relativistic and quantum size effects. The observed transition is due to a presence of quantum-well states [38–40] that are spin degenerate due to the conservation of the space-inversion symmetry if the whole film is considered. However, the analysis of the charge distribution inside the film and of the in-plane spin component perpendicular to the wave vector reveals a local SP (figure 5) and it was concluded that the spin property at the $\overline{\mathrm{M}}$ point is dominated by the parity effect [41].

So, very early, it appeared that the SP of the Bi surface states cannot be attributed solely to the conventional Rashba splitting as claimed in the first SARPES reports [40, 41]. Improved resolution in SARPES measurements allowed to prove that the in-plane SP is remarkably suppressed on a half of six elongated hole pockets of the surface states and that a giant out-of-plane SP is observed [42, 43]. These unconventional features are explained in terms of symmetry breaking and many-body effects, similarly to the Bi and Pb on Ag(1 1 1) surface alloy systems where the in-plane potential gradient [64] causes the out-of-plane SP [65].

For the sake of completeness, let us mention that there is a series of studies dealing with the Rashba effect at the Bi/Ag(1 1 1) interface. Bi is found to induce a giant spin splitting [66] that can be tuned in the surface alloy Bi_xPb_{1-x}/Ag(1 1 1) [67]. It enhances as well the electron-phonon coupling strength which is much stronger than either for the clean Ag(1 1 1) surface state or for bulk Ag [68].

Calculations explain the observed large enhancement of the Rashba splitting by the strong distortion of the surface-state wave function which is caused by the surface corrugation [69, 70]. In more detail, the experimentally observed anisotropy of the splitting can only be described if higher-order contributions to the Rashba–Bychkov Hamiltonian are included [71].

On decreasing the Bi film thickness, the SP at the $\overline{\mathrm{M}}$ point was found to be gradually reduced as a consequence of the quantum-well states influence (figure 6). It is has been demonstrated that the coupling between the Bi film and the Si(1 1 1) substrate is fairly weak [44], suggesting the nearly free-standing nature of the Bi film. The interface between Bi and Si can be regarded as a "bottom surface" (Si side) where Rashba states similar to those at the normal surface (vacuum side) would emerge due to the breaking of the space-inversion symmetry at the interface. These two Rashba states would have opposite spin directions because of the symmetry requirement. When the Bi film is thick enough, these states are independent from each other. Upon reducing film thickness, the wave functions of the two Rashba states start to overlap and hybridize, eventually leading to a substantially reduced in-plane component of the SP [44, 47].

3.3. Spin polarization – Spin-orbital entanglement

It seems opportune to remind here that information obtained from photoemission spectra is a function of intrinsic properties of the system under study. As a first approximation, the spin is preserved in the electric dipole transition. So, spin-resolved photoemission can extract the spin character of the electronic states and bring a new information in materials where the band structure is controlled only by exchange interaction. However, for materials where the SOC plays a significant role, as this is the case for Bi, the spin direction may depend on the position both in real space and momentum space, as well as on the symmetry of the states, since the spin is no longer a good quantum number [72, 73]. The experimental geometry, such as the light polarization and the incidence or emission angle, influences the measured SP in

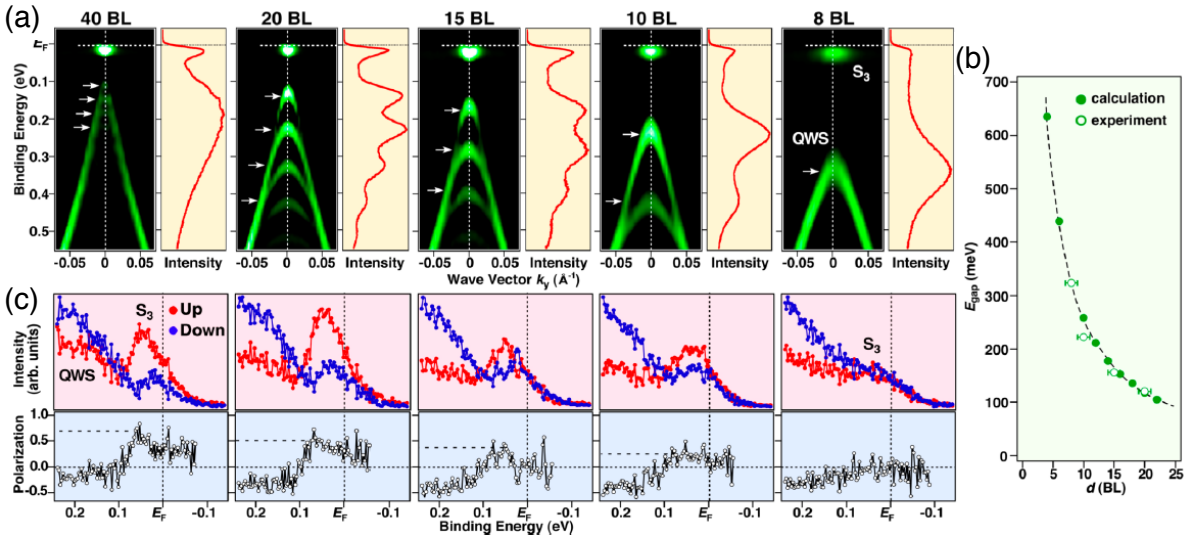

Figure 6. (a) Bi thickness dependence of the band dispersion (the second derivative with respect to energy of the energy distribution curves is shown) near the Fermi level (E_F) along the $\overline{M}$–$\overline{K}$ direction measured at 30 K on Bi/Si(1 1 1). Energy distribution curves at the $\overline{M}$ point are also shown for each thickness. (b) Comparison of the thickness dependence of the energy interval (E_{gap}) between the bottom of conduction the band [labelled S_3 in (a)] and the top of the quantum-well states (QWS) at the $\overline{M}$ point with that of the band calculation. (c) Corresponding spin-resolved energy distribution curves (top) and their spin polarization (bottom) in the vicinity of the $\overline{M}$ point. Reprinted with permission from [44]. Copyright 2012 American Chemical Society.

both magnitude and direction [74]. The SOC mixes states with different spin and orbital character and the light polarization selects the orbital character of the electronic states involved in the photoemission process. So, the spin information obtained from photoemission experiments on spin-orbit influenced surfaces has to be taken with precaution, while it remains reliable for states with pure symmetry [73]. Even if the mirror symmetry governs the spin orientation in the initial states, rotating the electric-field vector of the incident linearly polarized light can break the mirror symmetry of the experimental geometry, which leads to a specific SP of the photoelectrons.

The entangled spin-orbital textures have been first explored in TIs [75–78] and later in unoccupied bands of the Bi/Ag(1 1 1) surface alloy [73] and in elemental Bi [50]. Laser excited SARPES studies of the Bi(1 1 1) surface allow to establish a general description of the spin-orbital texture in even-odd parity symmetry. Moreover, a new concept has been developed to determine the phase of the photoemission dipole transition matrix element through the spin-dependent quantum interference, which relies on the spin-orbital-entanglement and the laser field [50].

3.4. Bismuth film as a topological insulator: theoretical approaches

TIs are bulk insulators which support protected boundary states [79, 80]. The easiest way to describe a TI is as an insulator that always has a metallic boundary when placed next to a vacuum or an "ordinary" insulator. These metallic boundaries originate from topological invariants, which cannot change as long as the material remains insulating. Nevertheless, these invariants do change in crossing the interface between topological and "ordinary" insulators, so by contradiction the surface cannot remain insulating [81]. In two dimensions, this phenomenon is called the quantum spin Hall effect and is distinguished by 1D chiral edge modes propagating along the perimeter of the system that are immune to non-magnetic disorder. It was first theoretically predicted for graphene with spin-orbit interaction included [82] and was further generalized to three dimensions [83–87].

Thin films are more relevant to actual device architecture. Efforts have been made to reduce the thickness of known bulk topological insulators [79, 80]. Benefits of a minimal film thickness include: i) bulk conduction and scattering caused by natural defects (a general issue) are minimized; ii) the band gap can be enhanced by quantum size effects; iii) discretization of the bulk bands can turn a semimetal (or a metal) into an insulator. The choice of available materials is thus substantially broadened. However, the usable film thickness has a natural lower limit below which the two film boundaries may be coupled by quantum tunnelling, so that a small, thickness-dependent, gap opens up at the Dirac point, cutting off the spin conduction.

The requirement of fine tuning the film thickness makes the experimental fabrication of 2D TIs rather difficult. Therefore, it is desirable to search for simpler materials with strong SOC. Bismuth thin films are candidates of choice. This initiated a large amount of theoretical studies concentrating on the (1 1 1) face [7, 88–107]. Rare are reports on other crystallographic faces. Non-trivial 2D TI phases in 2-BL and 4-BL Bi(1 1 0) have been reported by combining first-principles calculations and scanning tunnelling microscopy [108].

Another approach is the searching for new structural phases. *Ab initio* calculations demonstrate that Bi with the space group No. 139 (I4/mmm) is a topological crystalline insulator. This system takes advantage of dual protection: the Dirac cones are pinned at the high-symmetry points of the (0 0 1) surface; as a consequence they are protected by time-reversal symmetry and, even if in-plane mirror symmetry is broken at the surface, they can survive in the presence of a weak disorder [109].

When considering nanostructures, calculations suggest that the topological edge states of zigzag Bi(1 1 1) nanoribbon might be significantly tuned by H edge adsorption, the most remarkable effect being an increase by one order of magnitude of the Fermi velocity as the Dirac point is moved from the Brillouin zone boundary to the Brillouin zone centre, the real-space distribution of Dirac states being twice more delocalized [110].

Several band structure calculations based on on a first-principles have been published quite early because an effective single particle picture and the Bloch symmetry

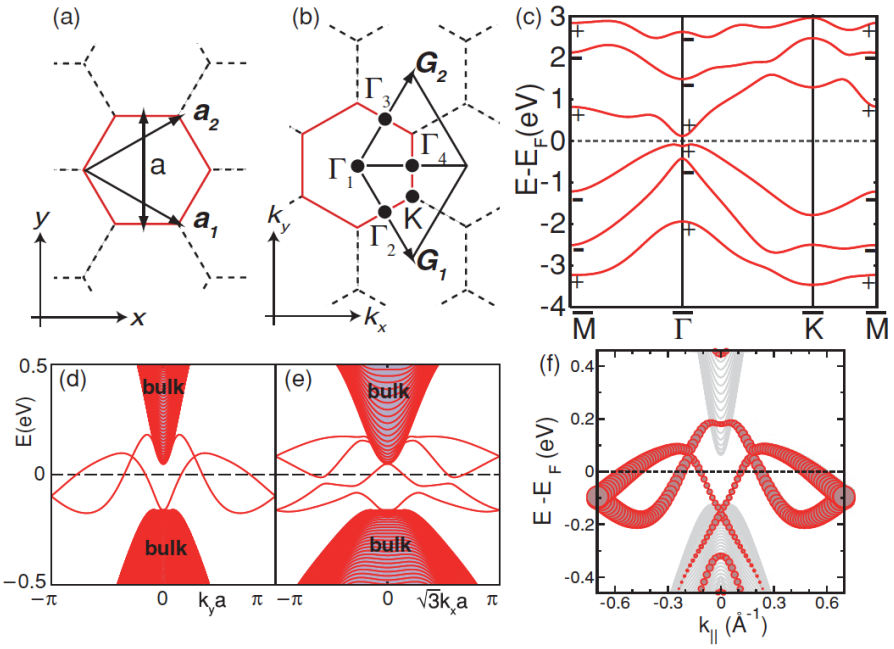

Figure 7. (a) Unit cell and lattice vectors, and (b) time-reversal invariant momenta (TRIMs) of a 1 bilayer Bi(1 1 1) film. The TRIMs consist of the Γ point and the three M points. (c) Bulk energy bands and the parity at the TRIMs for a 1 bilayer Bi(1 1 1) film. (d) and (e) Energy bands of the Bi(1 1 1) zigzag- and armchair-edge ribbons, respectively, with a width of 20 unit cells, calculated from the tight-binding model. (f) Energy bands of a eight-unit-cell-wide Bi(111) zigzag-edge ribbon from first-principles calculations. The size of the symbols corresponds to the weight of the states in the edge atoms. Reprinted figure with permission from [91]. Copyright (2011) by the American Physical Society.

still apply. In particular, density functional theory based calculations for Bi(1 1 1) free-standing monolayers and thin films predicted a topological behaviour of such films [90,91] (see e.g. figure 7).

The 1 BL Bi(1 1 1) film has a honeycomb structure, if one neglects the out-of-plane coordinate. Therefore, as in graphene, it is possible to refer to the two types of simple edge shapes as zigzag and armchair edges. Figures 7(d) and 7(e) show the energy bands of zigzag- and armchair-edge ribbons of the Bi(1 1 1) BL calculated in the tight-binding framework. In both figures, the number of Kramers pairs of edge states per one edge is odd, confirming that the 1 BL Bi(1 1 1) film is a quantum spin Hall system. Result from the tight-binding model [figure 7(d)] and that from a first-principles calculation [figure 7(f)] are in good agreement [91].

Further theoretical study [90] indicated a more complex behaviour of the Bi(1 1 1) films. The film below 4 BLs is an intrinsic 2D TI with a band structure consisting of "molecular orbital" levels without distinction between surface bands and bulk bands. Above 4 BLs, the band structure is made of surface bands superimposed onto 2D projected bulk bands. The projected 2D bulk bands still keep the non-trivial topology of a 2D TI with a sizeable gap, but the surface bands gradually appear in the middle of

the projected bulk band gap with increasing film thickness (see also [89]), leading to a semiconductor (1–4 BLs) to a semimetal (5–8 BLs) transition. It is proposed that the trivial metallic surface states can be removed by surface H adsorption which effectively converts the Bi films into true 2D TIs [89].

As it is demonstrated in this review, the SARPES plays a central role for the investigation of TIs and the closely related Rashba-type systems. Various experimental aspects of the spin polarised photoemission have been reviewed and discussed by Dil et al. [111]. The first-principles studies beyond the ground state, i.e. addressing spectroscopic properties and perhaps possible disorder/interdiffusion scenarios, are rare. The interpretation of the corresponding spectra is in general based only on the calculated bands [112] or Bloch spectral functions [64], respectively. So far, simplifying models have been used to discuss for example the origin of the SP monitored by SARPES [113]. The role of the divergence of the radiation vector potential at the surface and the possible connection between circular dichroism in ARPES and the SP have been investigated only recently for the Bi/Ag(1 1 1) Rashba system using a tight-binding model [114]. In spite of the considerable success of SARPES, the reliability of this method for the investigation of the spin properties of TI surfaces has been discussed in various experimental [115,116] and theoretical [113,117] studies. Part of these works involves the interpretation of the circular dichroism in the ARPES as the SP of Rashba split and topological surface states [115–117]. If this would be correct it can improve the efficiency of SP detection. Recent experimental and theoretical studies [118,119] clarified that measuring circular dichroism cannot replace the more demanding spin-resolved measurements which also calls the recent theoretical conclusions [114,120] into question. Generally speaking, spin-resolved photoemission does not allow directly identifying the measured SP to the initial states SP. The photoemission excitation process related aspects of measured SP have to be addressed within an *ab initio* study based on the one-step model of photoemission which accounts for all relativistic effects, the surface geometry as well as all matrix element effects at the same level [121,122]. In particular most of the theoretical analysis are based on very simplified approximations, e.g. free electron final state and normal emission geometry. This leads to various interpretations of the measured SP which might be misleading. The very few one-step model investigations on TIs together with the experiments on Rashba systems [73,123] clearly demonstrate the need for the support of theoretical investigations to deduce unambiguous information from experimental SARPES data. This holds in particular when the photon energy is varied over a wide range to change the probing depth [124,125].

3.5. Bismuth thin layers on topological insulators

All mentioned theoretical works clearly suggested topological properties of Bi to be reduced to one or several BLs. However experimentalists faced difficulties to verify it. No topological effects were reported experimentally on deposited BLs of Bi, probably because of its unique surface and interface properties [2]. As already mentioned, the

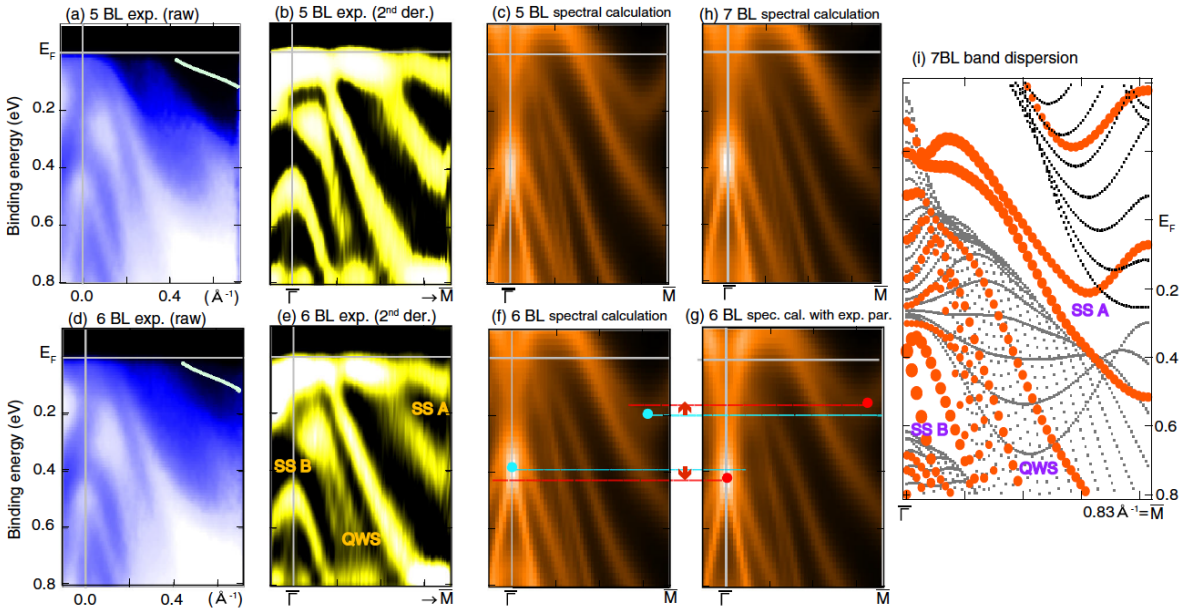

Figure 8. (a) Angle-resolved photoelectron spectroscopy (ARPES) image along the $\overline{\Gamma}$–$\overline{\mathrm{M}}$ direction of a 5 bilayers (BL) Bi(1 1 1) film on Bi_2Te_3 (raw data) and (b) its second derivative with respect to energy. (c) The calculated weighed spectral function (WSF) for a 5 BL strained Bi(1 1 1) film, which is the band dispersion weighed by the magnitude of the wave function localization at the topmost Bi BL. (d) Experimentally measured raw ARPES image and (e) its second derivative with respect to energy along the $\overline{\Gamma}$–$\overline{\mathrm{M}}$ direction of the 6 BL Bi(1 1 1) film on Bi_2Te_3. (f–g) The WSF for a 6 BL strained Bi(1 1 1) film [in (f) the optimized structure in the calculation is used, whereas in (g) the experimentally obtained lattice parameters are used; the arrows show the slight energy change]. (h) The WSF for a 7 BL strained Bi(1 1 1) film. (i) The band dispersion for the 7 BL strained Bi(1 1 1) film together with the bulk band projection (the size of the circles indicates the magnitude of the surface localization of the wave function; SS and QWS represent surface and quantum-well states, respectively). Reprinted figure with permission from [126]. Copyright (2012) by the American Physical Society.

initial growth of Bi on non lattice-matching substrates, namely on Si(111), typically resulted in a pseudocubic Bi(1 1 0) BL. Only upon additional deposition, Bi(1 1 1) begins to form, the film being presumably too thick to maintain the predicted states.

In order to circumvent the difficulties of preparing a single Bi BL on commonly used substrates, as Si(1 1 1), the straightforward idea is to realize the deposition directly on existing Bi-based TIs. Using such an approach problems connected with epitaxial growth can be solved in a simple way. Subsequently, the atomic and electronic structures of Bi(1 1 1) films grown on Bi_2Te_3, Bi_2Se_3, Bi_2Te_2Se and $Bi_2Te_{2.4}Se_{0.6}$ [76,126–132] have been determined by means of several techniques, namely ARPES, and compared to first-principles calculations. Some of the results have been reviewed in [27].

ARPES studies using TIs as a substrate do not allow however to form a conclusive assessment because the similarities in the electronic structures of the Bi film and of the substrate preclude disentangling their respective contributions to the data.

One of the driving forces of the topological transition is the strain due to the lattice mismatch. For instance, when the Bi(1 1 1) film is grown on Bi_2Te_3(1 1 1), it is horizontally contracted and vertically expanded compared to the bulk values. ARPES studies show that this lattice distortion induces a change in the surface state band dispersion and the theoretical calculation reveals that 3D Bi becomes topological (figure 8). This can be recognized in edge state dispersion [see figure 8(i)] [126]. While one of the surface states connects to the valence bands at both the $\overline{\Gamma}$ point and the $\overline{\mathrm{M}}$ point, the other one connects to the valence band at the $\overline{\Gamma}$ point and the conduction band at the $\overline{\mathrm{M}}$ point, a characteristic feature of topological edge states.

When measuring the spin texture, this one is the same for the intrinsic Dirac cone of Bi_2Se_3 or Bi_2Te_3 surface states, the extrinsic Dirac cone of Bi BL induced by the Rashba effect and the hybridized Dirac cone between the former two states [76]. However, according to [130], the strong hybridization between Bi and the Dirac-cone states in Bi_2Te_3 observed in 1 BL film does not occur for other thicknesses. On the contrary, in another study [131], a direct experimental signature has been found that even a thicker film, 30 nm Bi(1 1 1)/Bi_2Te_3, can be topologically non-trivial in three dimension. At the same time the authors concede that the origin of these non-trivial properties is not yet understood and needs further investigations.

Slightly more convincing confirmation is brought up using real-space resolution of scanning tunnelling microscopy and spectroscopy (STM/STS). The edge states can be directly observed on single BL Bi(1 1 1) islands, in both real and energy spaces, which are grown on clean Bi_2Te_3 and Bi(1 1 1)-covered Bi_2Te_3 substrates [128].

A similar STM study on a well-ordered single Bi BL with zigzag edges, grown epitaxially on a cleaved Bi_2Te_2Se crystal represents a clear real space observation of the edge electronic states of a 2D TI, correspondin,g to a quantum spin Hall state [129]. It is shown that the strong interfacial interaction with the substrate induces a large splitting of the degenerate valence bands of Bi(1 1 1) and the band hybridization with those of the substrate. The hybridization leads to the formation of a characteristic interfacial state and a small hybridization energy gap above the Fermi level for the Bi film. Irrespective of such a strong interaction with the substrate, the band inversion of the Bi film and the edge state are shown to be robust. The edge state along the zigzag edge exhibits a substantial energy shift. This edge state signature was unambiguously resolved in the STS spectra and spatial maps [129] (figure 9). But, according to the authors, the topological or helical nature of the edge state has to be confirmed further, for example, by a spin-polarized tunnelling experiment.

3.6. Bismuth thin layers: edge states

Another approach in the quest of topological properties of Bi films is to continue auscultating the edge states on substrates that are not TIs; for instance, looking at terraces on top of a Bi monocrystal [48, 133–136]. As indicated by theoretical considerations some years ago, a 3D Bi crystal is topologically trivial [137] whereas a

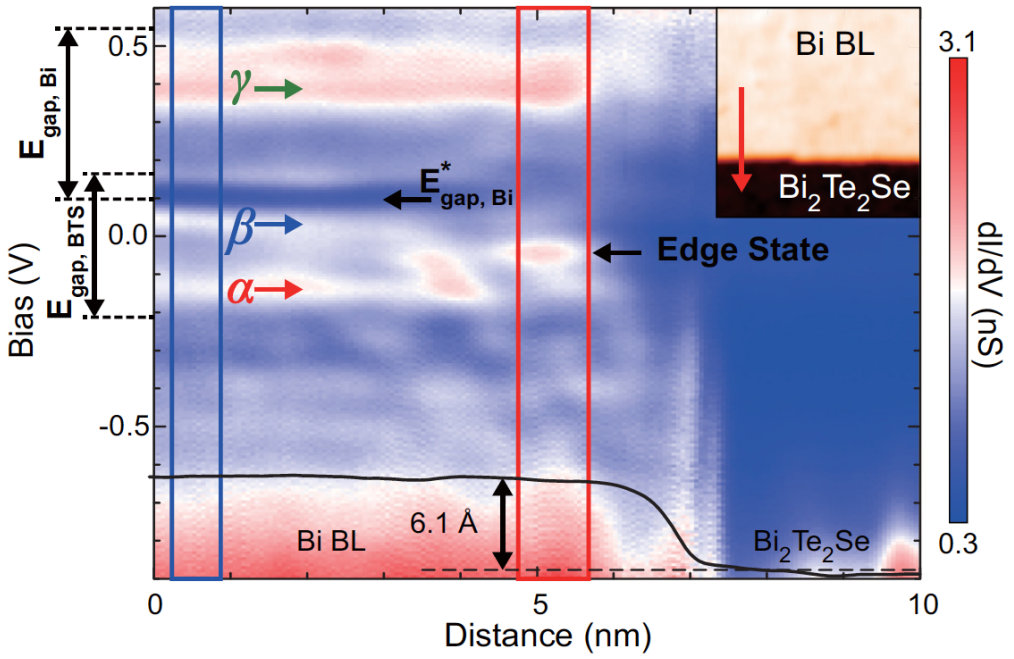

Figure 9. Two-dimensional plot of the scanning tunnelling spectroscopy (STS) ($\mathrm{d}I/\mathrm{d}V$) line scan along the arrow indicated in the inset, that crosses one zigzag edge of a Bi(1 1 1) bilayer island. The topography image in the inset covers a $20 \times 20\,\mathrm{nm}^2$ area. Three major spectral features of the Bi(1 1 1) bilayer film and the distinct edge state are indicated by arrows. The topographic profile obtained during the STS measurement is given at the bottom of the figure. Reprinted figure with permission from [129], where further details can be found. Copyright (2014) by the American Physical Society.

non-trivial $\mathbb{Z}_2$ topology of Bi(1 1 1) thin films can persist even in the case of multi-bilayer thick films [90]. The thickness limit where topological properties vanish is not clearly predicted by theory and up to date reported experimental results are contradictory.

The question arises whether terraces present on the surface and/or vicinal surfaces could harbour a quantum spin Hall effect. The first indication in this direction was discovered on the (1 1 4) surface of a Bi bulk crystal which was found to support a quasi 1D, metallic surface state. The electronic structure at the Fermi level consists of only two crossings with opposite spin and $\mathbf{k}$, and therefore strongly resembles the edge states in the quantum spin Hall effect [133].

STM based mechanical and electrical characterization techniques, bring as well evidence of the quantum spin Hall phase in a two-dimensional crystal produced the mechanical exfoliation of a Bi(1 1 1) BL [138]. Electrical conductance measurements of Bi nanocontacts created by repeated tip-surface indentation at temperatures of 4 K and 300 K testify the presence of plateaus of conductance $G_0 = 2e^2/h$ at room temperature.

Similarly, later theoretical study claimed that all of the predicted topological properties of the edge states of a free-standing Bi BL will be present even on top of a cleaved Bi(1 1 1) bulk crystal which was confirmed by STM experiments [134]. At the

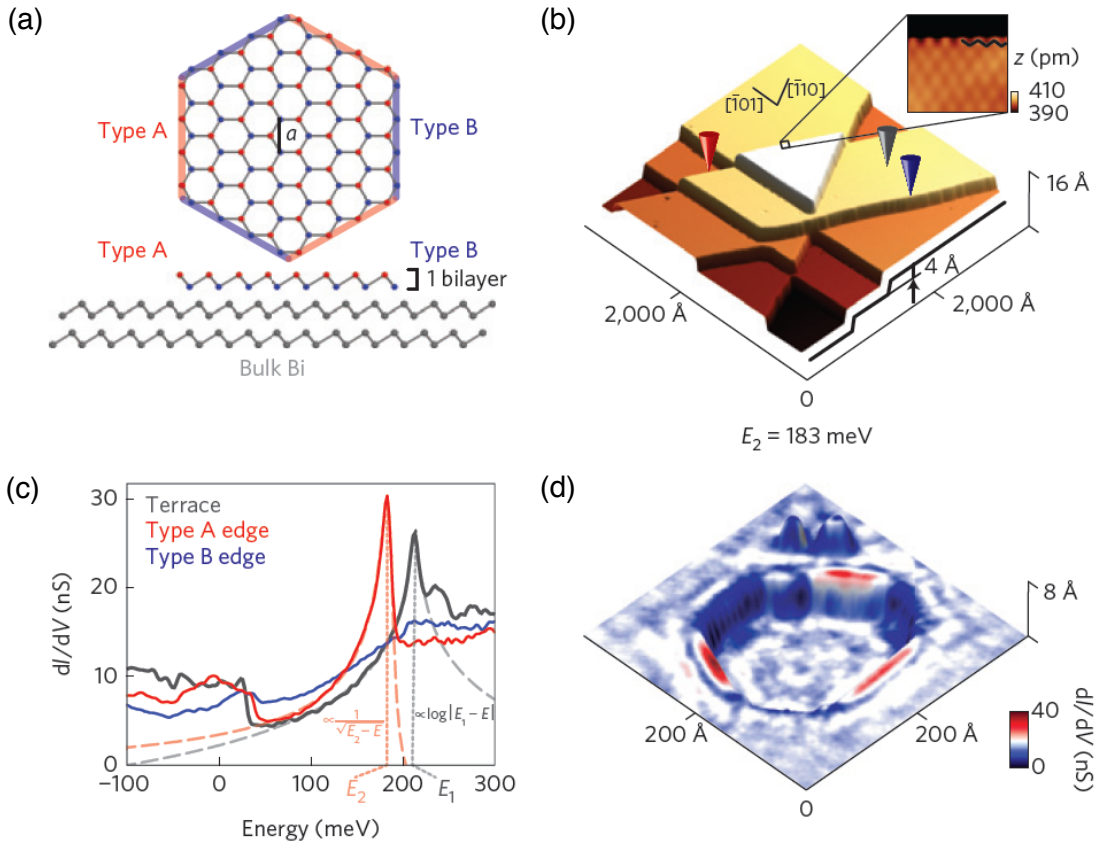

Figure 10. Edges of Bi bilayer islands on a Bi crystal surface. (a): Schematics of the Bi bilayer atomic structure (upper panel: top view; lower panel: side view). Type A and type B edges, i.e. edges terminated by atoms close to the vacuum and to the substrate underneath, are shown by the red and blue lines, respectively. The Bi lattice constant is 4.5 Å. (b) Topographic image of the Bi(1 1 1) single-crystal surface. The height of the Bi bilayer islands is 4.0 Å (line profile on the right). The inset shows a 30×30 Å^2 atomically resolved topographic image of a zigzag edge. (c) Point spectroscopy at the two different types of edge A (red line) and B (blue line) and on the surface away from the edges (grey line). Whereas the spectrum on the type A edges shows a maximum at $E_2 = 183$ meV that can be fitted to the expected 1D density of states (dashed orange line), the spectrum on the type B edge is almost featureless. (d) Topography close to the hexagonal diatomic depression, false-coloured with differential conductance at $E_2 = 183$ meV. A high conductance (in red) is observed at every other edge of a hexagonal pit-like defect. Reprinted by permission from Springer Nature: Nature Physics (reference [134]), Copyright (2014).

same time the authors of reference [134] point out that the presence of such topological 1D edge states (see figure 10) of the Bi BL does not imply that the bulk Bi crystal is topologically non-trivial. Similar findings were supported by a more recent work on thick Bi(1 1 1) films grown on a Si substrate [135].

On the other hand, Bi thin films on Si(1 1 1) fabricated with many edge structures exhibit 1D states with a giant Rashba effect and a sizeable out-of-plane SP but are found to have a topologically trivial nature [48]. These findings are supported by a

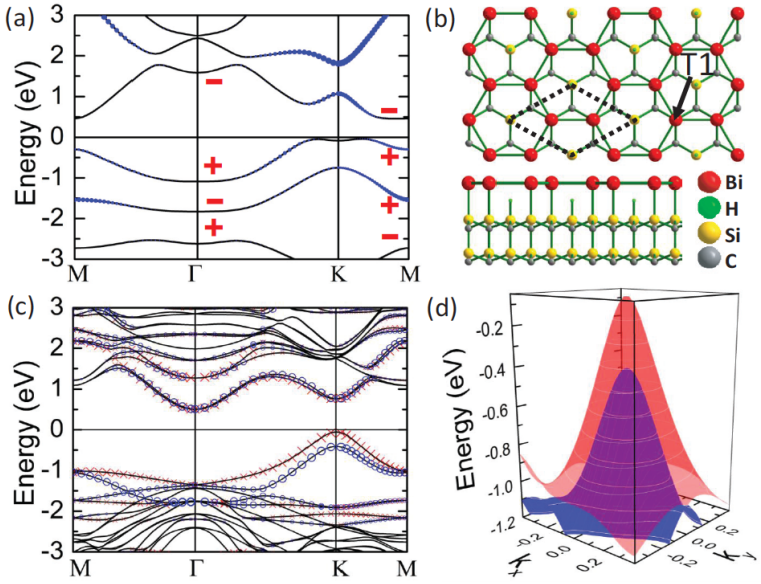

Figure 11. (a) Band structure of the free-standing Bi thin film in planar honeycomb structure ith a lattice constant at 5.35 Å. (b) Atomic structure of Bi honeycomb on a SiC(0001)-($\sqrt{3}\times\sqrt{3}$) substrate. (c) Band structure of the Bi honeycomb on SiC(0 0 0 1)-($\sqrt{3}\times\sqrt{3}$). Red crosses and blue circles identify Bi-derived states with opposite spins. (d) Blow-up of the band structure of (c) around the K point. Red and blue colours refer to opposite spin polarizations of the bands. Reprinted figure with permission from [93]. Copyright (2013) by the American Physical Society.

later calculations [136] where the 1D band structure of step edges of Bi(1 1 1) films was explicitly studied as a function of the film thickness. It unambiguously appeared that the dispersion of step-edge states reflects the topological nature of the underlying films, rather than indicating the existence of topological edge states along step edges on surfaces of a bulk Bi(1 1 1) crystal or a sufficiently thick Bi(1 1 1) film. The trivial step-edge states have the spin splitting of 1D Rashba bands.

Looking at all these aforementioned results, it appears that the true nature of the edge states is still waiting to be elucidated in more detail.

3.7. Bismuthene: the ultimate layer

Following the prediction of topological properties for a free-standing single BL of Bi [7, 91] many theoretical studies proposed suitable substrates allowing building real films with a stable structure [93, 95, 97–100, 102, 103, 105].

At this stage, it is useful noting that the terminology in literature slightly evolved and in analogy with graphene the names of single-layered materials are often extended with suffix "-ene" [96]. So, here, we will speak about bismuthene and, similarly to hydrogenated graphene or graphane, we may refer to hydrogen terminated bismuthene as bismuthane [100]. In the same logic, the porous allotrope of a Bi monolayer is denominated as bismuthylene [105]. Electronic structure of free-standing bismuthene

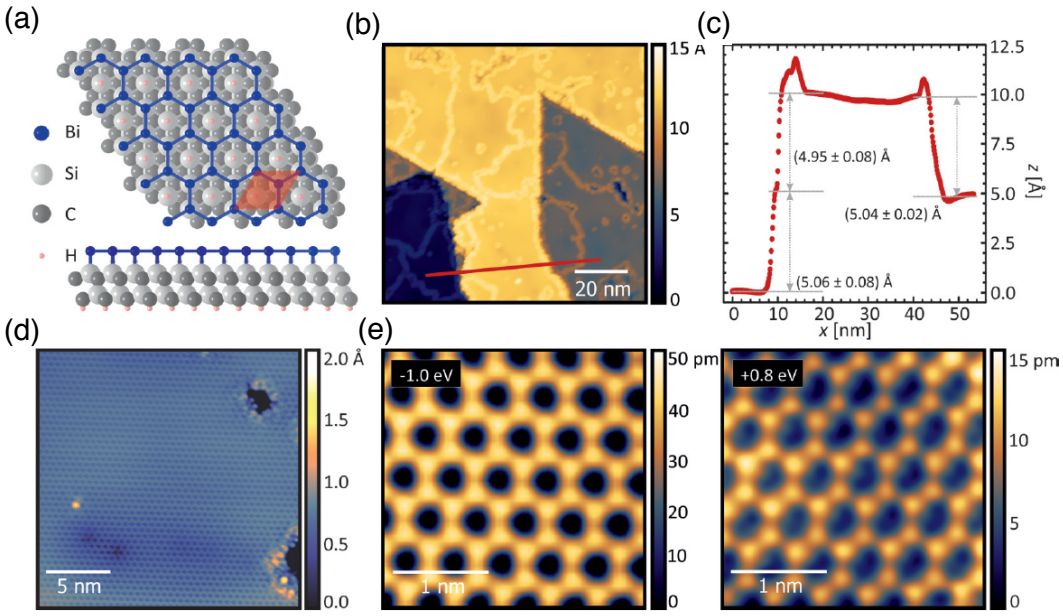

Figure 12. Bismuthene on SiC(0 0 0 1) structural model. (a) Sketch of a bismuthene layer placed on the threefold-symmetric SiC(0 0 0 1) substrate in a $(\sqrt{3} \times \sqrt{3})R30°$ superstructure. (b) Topographic scanning tunnelling microscopy (STM) map showing that bismuthene fully covers the substrate (the flakes are of ~ 25 nm extent, limited by domain boundaries). (c) Substrate step height profile, taken along the red line in (b), corresponding to SiC steps. (d) The honeycomb pattern as seen on smaller scan frames. (e) Close-up STM images for occupied and empty states (left and right panel, respectively) that confirm the formation of Bi honeycombs. Reprinted with permission from [140]. Copyright 2017 American Association for the Advancement of Science.

has been addressed in [101, 104] and that of double layer bismuthene in [106]. Some aspects of single-layer films of the group V elements, the so-called pnictogens, have been reviewed in [139].

Theoretical studies show that the Bi(1 1 1) film on a suitable substrate represents an interesting case with an intermediate inter-bilayer coupling strength and where the strain induced by a substrate can as well induce topological properties [93]. The authors define here a measure of band inversion strength which provides a basis for constructing a topological phase diagram of Bi BLs for assessing the robustness of the non-trivial topological phases as a function of strain and/or the size of buckling. The analysis indicates that insulating and weakly interacting substrate hexagonal-BN could be a good substrate candidate for a nearly free-standing 2D quantum spin Hall phase of the Bi BL film.

Turning to larger strains or lattice constants where the Bi BL assumes the planar honeycomb structure, the candidate substrate for support is SiC(0 0 0 1)-$(\sqrt{3} \times \sqrt{3})$ with the Bi lattice constant of 5.35 Å (figure 11). The substrate induces pronounced spin-splitting of bands around the K point [figure 11(d)]. This planar Bi honeycomb has

been previously thought to be a trivial insulator [93]. However, in a later study by the same authors [100], it has been reevaluated and finally shown that the substrate forces this trivial film into becoming non-trivial. The underlying physical mechanism is due to an orbital filtering effect of the substrate [98].

Following this prediction, it was possible to grow the first Bi BL on a SiC(0 0 0 1) substrate [140]. This substrate is not only stabilizing the quasi-2D TI but also plays a pivotal role for achieving the large gap, with the strong on-site SOC coming directly into play. The observed structure has a $(\sqrt{3} \times \sqrt{3})R30^\circ$ superstructure of Bi atoms in honeycomb geometry. The resulting lattice constant of 5.35 Å is significantly larger than that of buckled Bi(1 1 1) BLs. This induces a fully planar configuration of the honeycomb layer. Although the topological character of the edge states has experimentally yet to be established, i.e. by a direct transport measurement of the quantum spin Hall effect with its universal quantized conductance, the agreement between experimental evidence and theoretical prediction already strongly suggests that the quantum spin Hall scenario in Bi/SiC is valid.

3.8. Possible future prospects

As mentioned in section 3.4, checking theoretical predictions concerning thin film topological phases is often a challenge hard to overcome experimentally. We saw for instance that this is the case of the ultimate Bi layer (section 3.7). Another example is a new structural phase of Bi-139(001) (see section 3.4) that is a topological crystalline insulator taking advantage of dual protection [109].

The main origin of the difficulty to fabricate such systems lies in the limitation of the available growth techniques.

Embedding Bi atoms in an appropriate structure appears to be one of possible approaches to circumvent these difficulties, as it has been shown for the InBi crystal. A thorough analysis combining ARPES measurements and fully-relativistic *ab initio* electronic band calculations of InBi(0 0 1), grown on the InAs(1 1 1)-A surface, indicates that the topmost Bi BL has the same structure as Bi in the space group No. 139 configuration [141]. Nonetheless, the mirror plane parallel to the (0 0 1) plane for Bi-139 does not exist within InBi, which indicates that only a single BL of Bi-139 has been created. However, the general surface symmetries of the systems are the same: both $\overline{\Gamma M}$ and $\overline{\Gamma X}$ are mirror planes for both InBi(0 0 1) and Bi-139(0 0 1). Consequently, the topological states are protected by both, by time-reversal and discrete rotational symmetry [142].

The InBi crystal structure in the [0 0 1] direction can be seen as a stacking of [Bi–(2 In)–Bi] trilayers, with a Bi excess layer on the top of the surface [see figure 13(b)]. Bloch spectral function depicting the general band dispersion around the $\overline{M}$ point, where the Dirac point is located, is shown in figure 13(c). The surface topological states are originating from the p_z orbitals of the excess Bi atomic layer and they resonantly propagate via the bottom Bi atoms of the trilayers down to the bulk. This is shown in

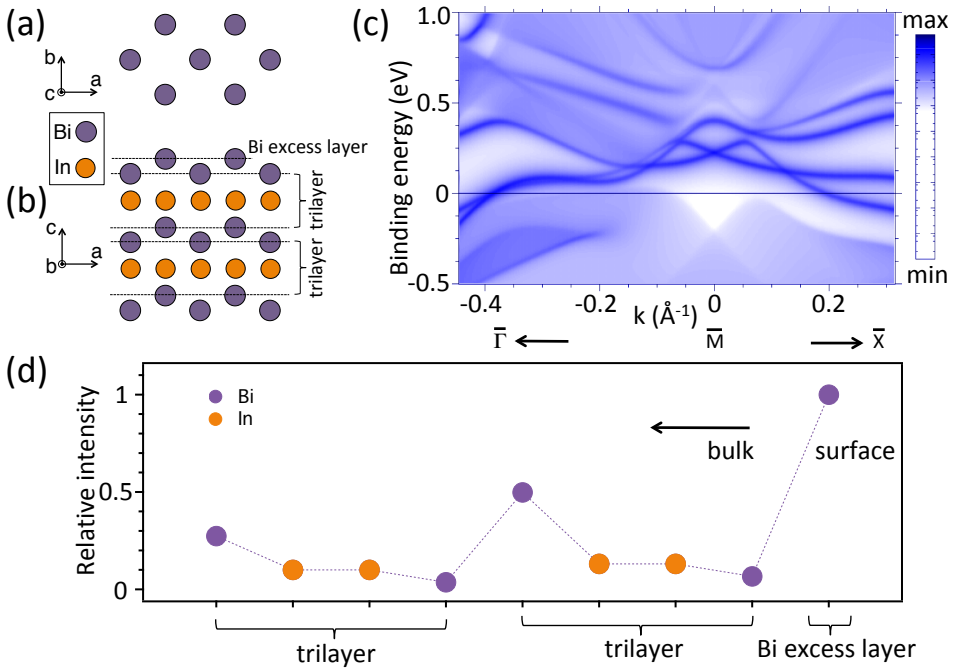

Figure 13. (a) Top- and (b) side-view of the InBi crystal in the [0 0 1] direction. The crystal can be seen as a stack of Bi–In–Bi trilayers terminated by an excess Bi layer on the surface. (c) Bloch spectral function depicting (in logarithmic colour scale) the general band dispersion around the $\overline{\mathrm{M}}$ point, where the Dirac point is situated. (d) Normalized intensities taken at the Dirac point and plotted from the excess layer towards the bulk of the crystal. For clarity, the intensities of both In atoms in the indium layer are shown. From [141].

figure 13(d), where the normalized intensities are taken at the Dirac point and plotted from the excess layer towards the bulk of the crystal.

This experimental realization of a theoretically predicted Bi topological crystalline insulator with outstanding properties opens the gate for future developments in the band-gap engineering of devices.

4. Summary

Topologically ordered phases of matter have recently received considerable attention both for their intrinsic physical interest and for the paths they may open towards technological breakthroughs. A great deal of attention has been placed on Bi-based systems because of the strong spin-orbit coupling of this heavy element, which could lead to get a large Rashba spin splitting. This, in combination with topological surface states, might lead to new developments in spintronics. In this contribution, an attempt has been made to summarize the present status of the research in this field as well as to present some ongoing research advances. It is underlined that, despite the availability of many theoretical predictions for topological phases in thin films, elaborating these films "in real life" is far from easy. Nevertheless, in the light of the progress already made,

we hope that this short review will stimulate new efforts in the practical realization of theoretically suggested systems.

Acknowledgments

JM and LN would like to thank the CEDAMNF (CZ.02.1.01/0.0/0.0/15_003/0000358) co-funded by the ERDF as part of the Ministry of Education, Youth and Sports of Czech Republic.

References

[1] Rumble J R (ed) 2018 *CRC Handbook of Chemistry and Physics* 99th ed (Boca Raton, FL: CRC Press)
[2] Hofmann Ph 2006 *Prog. Surf. Sci.* **81** 191
[3] Otani Y, Shiraishi M, Oiwa A, Saitoh E and Murakami S 207 *Nat. Phys.* **13** 829
[4] Loss D and DiVincenzo D P 1998 *Phys. Rev. A* **57** 120
[5] Rashba E I 1960 *Sov. Phys. Solid State* **2** 1109 [*Fiz. Tverd. Tela (Leningrad)* 1960 **2**, 1224]
[6] Bihlmayer G, Rader O and Winkler R 2015 *New J. Phys.* **17** 050202 [See also the supplementary information available at `stacks.iop.org/NJP/17/050202/mmedia`]
[7] Murakami S 2006 *Phys. Rev. Lett.* **97** 236805
[8] Hüfner S 2003 *Photoelectron Spectroscopy* (Berlin: Springer)
[9] Hüfner S (ed) 2007 *Very High Resolution Photoelectron Spectroscopy* (*Lecture Notes in Physics* vol 717) (Berlin: Springer)
[10] Suga S and Sekiyama A (eds) 2014 *Photoelectron Spectroscopy* (*Springer Series in Optical Sciences* vol 176) (Berlin: Springer)
[11] Seddon E A 2016 Spin-resolved valence photoemission *Handbook of Spintronics* vol 1 ed Xu Y, Awschalom D and Nitta J (Dordrecht: Springer Science+Business Media) chap 31, p 1243
[12] Mönig H, Sun J, Koroteev Yu M, Bihlmayer G, Wells J, Chulkov E V, Pohl K and Hofmann Ph 2005 *Phys. Rev. B* **72** 085410
[13] Ogrin Y F, Lutskii V N and Elinson M I 1966 *JETP Lett.* **3** 71 [*Pis'ma Zh. Eksp. Teor. Fiz.* 1966 **3** 114]
[14] Jezequel G, Petroff Y, Pinchaux R and Yndurain F 1986 *Phys. Rev. B* **33** 4352
[15] Patthey F, Schneider W-D and Micklitz H 1994 *Phys. Rev. B* **49** 11293
[16] Tanaka A, Hatano M, Takahashi K, Sasaki H, Suzuki S and Sato S 1999 *Phys. Rev. B* **59** 1786
[17] Hengsberger M, Segovia P, Garnier M, Purdie D and Baer Y 2000 *Eur. Phys. J. B* **17** 603
[18] Ast C R and Höchst H 2001 *Phys. Rev. Lett.* **87** 177602
[19] Ast C R and Höchst H 2002 *Phys. Rev. B* **66** 125103
[20] Ast C R and Höchst H 2003 *Phys. Rev. B* **67** 113102
[21] Ast C R and Höchst H 2004 *Phys. Rev. B* **70** 245122
[22] Petersen L and Hedegård P 2000 *Surf. Sci.* **459** 49
[23] Manchon A, Koo H C, Nitta J, Frolov S M and Duine R A 2015 *Nat. Mater.* **14** 871
[24] Koroteev Yu M, Bihlmayer G, Gayone J E, Chulkov E V, Blügel S, Echenique P M and Hofmann Ph 2004 *Phys. Rev. Lett.* **93** 046403
[25] Liu Y and Allen R E 1995 *Phys. Rev. B* **52** 1566
[26] Kimura A, Krasovskii E E, Nishimura R, Miyamoto K, Kadono T, Kanomaru K, Chulkov E V, Bihlmayer G, Shimada K, Namatame H and Taniguchi M 2010 *Phys. Rev. Lett.* **105** 076804
[27] Gao C-L, Dong Q, Liu C-H, Jia J-F and Liu F 2013 *Chin. Phys. B* **22** 67304
[28] Okuda T and Kimura A 2013 *J. Phys. Soc. Jpn.* **82** 021002

[29] Perfetti L, Faure J, Papalazarou E, Mauchain J, Marsi M, Goerbig M O, Taleb-Ibrahimi A and Ohtsubo Y 2015 *J. Electron. Spectrosc. Relat. Phenom.* **201** 60

[30] Hirahara T 2015 *J. Electron. Spectrosc. Relat. Phenom.* **201** 98

[31] Ren Y, Qiao Z and Niu Q 2016 *Rep. Prog. Phys.* **79** 066501

[32] Bian G, Wang X, Kowalczyk P J, Maerkl T, Brown S A and Chiang T-C 2017 *J. Phys. Chem. Solids* in press

[33] Tanaka A, Hatano M, Takahashi K, Sasaki H, Suzuki S and Sato S 1999 *Surf. Sci.* **433-435** 647

[34] Nagao T, Doi T, Sekiguchi T and Hasegawa S 2000 *Jpn. J. Appl. Phys., Part 1* **39** 4567

[35] Yaginuma S, Nagao T, Sadowski J T, Pucci A, Fujikawa Y and Sakurai T 2003 *Surf. Sci.* **547** L877

[36] Payer T, Klein C, Acet M, Ney V, Kammler M, Meyer zu Heringdorf F-J and Horn-von Hoegen M 2012 *Thin Solid Films* **520** 6905

[37] Nagao T, Sadowski J T, Saito M, Yaginuma S, Fujikawa Y, Kogure T, Ohno T, Hasegawa Y, Hasegawa S and Sakurai T 2004 *Phys. Rev. Lett.* **93** 105501

[38] Hirahara T, Nagao T, Matsuda I, Bihlmayer G, Chulkov E V, Koroteev Yu M, Echenique P M, Saito M and Hasegawa S 2006 *Phys. Rev. Lett.* **97** 146803

[39] Hirahara T, Nagao T, Matsuda I, Bihlmayer G, Chulkov E V, Koroteev Yu M and Hasegawa S 2007 *Phys. Rev. B* **75** 035422

[40] Hirahara T, Miyamoto K, Matsuda I, Kadono T, Kimura A, Nagao T, Bihlmayer G, Chulkov E V, Qiao S, Shimada K, Namatame H, Taniguchi M and Hasegawa S 2007 *Phys. Rev. B* **76** 153305

[41] Hirahara T, Miyamoto K, Kimura A, Niinuma Y, Bihlmayer G, Chulkov E V, Nagao T, Matsuda I, Qiao S, Shimada K, Namatame H, Taniguchi M and Hasegawa S 2008 *New J. Phys.* **10** 083038

[42] Takayama A, Sato T, Souma S and Takahashi T 2011 *Phys. Rev. Lett.* **106** 166401

[43] Miyahara H, Maegawa T, Kuroda K, Kimura A, Miyamoto K, Namatame H, Taniguchi M and Okuda T 2012 *e-J. Surf. Sci. Nanotechnol.* **10** 153

[44] Takayama A, Sato T, Souma S Oguchi T and Takahashi T 2012 *Nano Lett.* **12** 1776

[45] Lükermann D, Banyoudeh S, Brand C, Sologub S, Pfnür H and Tegenkamp C 2014 *Surf. Sci.* **621** 82

[46] Takayama A, Sato T, Souma S and Takahashi T 2014 *New J. Phys.* **16** 055004

[47] Takayama A, Sato T, Souma S and Takahashi T 2015 *J. Electron. Spectrosc. Relat. Phenom.* **201** 105

[48] Takayama A, Sato T, Souma S, Oguchi T and Takahashi T 2015 *Phys. Rev. Lett.* **114** 066402

[49] Matetskiy A V, Bondarenko L V, Tupchaya A Y, Gruznev D V, Eremeev S V, Zotov A V and Saranin A A 2017 *Appl. Surf. Sci.* **406** 122

[50] Yaji K, Kuroda K, Toyohisa S, Harasawa A, Ishida Y, Watanabe S, Chen C, Kobayashi K, Komori F and Shin S 2017 *Nat. Commun.* **8** 14588

[51] Hatta S, Ohtsubo Y, Miyamoto S, Okuyama H and Aruga T 2009 *Appl. Surf. Sci.* **256** 1252

[52] Nicolaï L, Mariot J-M, Djukic U, Wang W, Heckmann O, Richter M C, Kanski J, Leandersson M, Sadowski J, Balasubramanian T, Vobornik I, Fujii J, Braun J, Ebert H, Minár J and Hricovini K 2018 arXiv:1807.00306v1

[53] Richter M C, Mariot J-M, Gafoor M A, Nicolaï L, Heckmann O, Djukic U, Ndiaye W, Vobornik I, Fujii J, Barrett N, Feyer V, Schneider C M and Hricovini K 2016 *Surf. Sci.* **651** 147

[54] Song F, Wells J W, Jiang Z, Saxegaard M and Wahlström E 2015 *ACS Appl. Mater. Interfaces* **7** 8525

[55] Jankowski M, Kamiński D, Vergeer K, Mirolo M, Francesco C, Rijnders G and Bollmann T R J 2017 *Nanotechnology* **28** 155602

[56] Bollmann T R J, van Gastel R, Zandvliet H J W and Poelsema B 2011 *Phys. Rev. Lett.* **107** 176102

[57] Mathias S, Ruffing A, Deicke F, Wiesenmayer M, Sakar I, Bihlmayer G, Chulkov E V, Koroteev

Yu M, Echenique P M, Bauer M and Aeschlimann M 2010 *Phys. Rev. Lett.* **104** 066802
[58] Kawakami N, Lin C L, Kawahara K, Kawai M, Arafune R and Takagi N 2017 *Phys. Rev. B* **96** 205402
[59] Hoffman C A, Meyer J R, Bartoli F J, Di Venere A, Yi X J, Hou C L, Wang H C, Ketterson J B and Wong G K 1993 *Phys. Rev. B* **48** 11431
[60] Lutskii V N 1965 *Sov. Phys. JETP Lett.* **2** 245 [*Pis'ma Zh. Eksp. Teor. Fiz.* 1965 **2** 391]
[61] Sandomirskiĭ V B 1967 *J. Exp. Theor. Phys.* **25** 101 [*Zh. Eksp. Teor. Fiz.* 1967 **52** 158]
[62] Xiao S, Wei D and Jin X 2012 *Phys. Rev. Lett.* **109**(16) 166805
[63] Winkler R 2003 *Spin–Orbit Coupling Effects in Two-Dimensional Electron and Hole Systems* (*Springer Tracts in Modern Physics* vol 191) (Berlin: Springer)
[64] Ast C R, Wittich G, Wahl P, Vogelgesang R, Pacilé D, Falub M C, Moreschini L, Papagno M, Grioni M and Kern K 2007 *Phys. Rev. B* **75** 201401
[65] Meier F, Dil H, Lobo-Checa J, Patthey L and Osterwalder J 2008 *Phys. Rev. B* **77** 165431
[66] Ast C R, Henk J, Ernst A, Moreschini L, Falub M C, Pacilé D, Bruno P, Kern K and Grioni M 2007 *Phys. Rev. Lett.* **98** 186807
[67] Ast C R, Pacilé D, Moreschini L, Falub M C, Papagno M, Kern K, Grioni M, Henk J, Ernst A, Ostanin S and Bruno P 2008 *Phys. Rev. B* **77** 081407
[68] Guan D, Bianchi M, Bao S, Perkins E, Meier F, Dil J H, Osterwalder J and Hofmann Ph 2011 *Phys. Rev. B* **83** 155451
[69] Bihlmayer G, Blügel S and Chulkov E V 2007 *Phys. Rev. B* **75** 195414
[70] Bian G, Wang X, Miller T and Chiang T-C 2013 *Phys. Rev. B* **88** 085427
[71] Vajna Sz, Simon E, Szilva A, Palotas K, Ujfalussy B and Szunyogh L 2012 *Phys. Rev. B* **85** 075404
[72] Yazyev O V, Moore J E and Louie S G 2010 *Phys. Rev. Lett.* **105** 266806
[73] Wissing S N P, Schmidt A B, Mirhosseini H, Henk J, Ast C R and Donath M 2014 *Phys. Rev. Lett.* **113** 116402
[74] Henk J, Scheunemann T, Halilov S V and Feder R 1996 *J. Phys.: Condens. Matter* **8** 47
[75] Jozwiak C, Park C-H, Gotlieb K, Hwang C, Lee D-H, Louie S G, Denlinger J D, Rotundu C R, Birgeneau R J, Hussain Z and Lanzara A 2013 *Nat. Phys.* **9** 293
[76] Miao L, Wang Z F, Yao M-Yu, Zhu F, Dil J H, Gao C L, Liu C, Liu F, Qian D and Jia J-F 2014 *Phys. Rev. B* **89** 155116
[77] Zhu Z-H, Veenstra C N, Zhdanovich S, Schneider M P, Okuda T, Miyamoto K, Zhu S-Y, Namatame H, Taniguchi M, Haverkort M W, Elfimov I S and Damascelli A 2014 *Phys. Rev. Lett.* **112** 076802
[78] Kuroda K, Yaji K, Nakayama M, Harasawa A, Ishida Y, Watanabe S, Chen C-T, Kondo T, Komori F and Shin S 2016 *Phys. Rev. B* **94** 165162
[79] Hasan M Z and Kane C L 2010 *Rev. Mod. Phys.* **82** 3045
[80] Qi X-L and Zhang S-C 2011 *Rev. Mod. Phys.* **83** 1057
[81] Moore J E 2010 *Nature* **464** 194
[82] Kane C L and Mele E J 2005 *Phys. Rev. Lett.* **95** 226801
[83] Fu L, Kane C L and Mele E J 2007 *Phys. Rev. Lett.* **98** 106803
[84] Zhang H, Liu C-X, Qi X-L, Dai X, Fang Z and Zhang Z-S 2009 *Nat. Phys.* **5** 438
[85] Hsieh D, Qian D, Wray L, Xia Y, Hor Y S, Cava R J and Hasan M Z 2008 *Nature* **452** 970
[86] Moore J E 2009 *Nat. Phys.* **5** 378
[87] Xia Y, Qian D, Hsieh D, Wray L, Pal A, Lin H, Bansil A, Grauer D, Hor Y S, Cava R J and Hasan M Z 2009 *Nat. Phys.* **5** 398
[88] Fukui T and Hatsugai Y 2007 *J. Phys. Soc. Jpn.* **76** 053702
[89] Koroteev Yu M, Bihlmayer G, Chulkov E V and Blügel S 2008 *Phys. Rev. B* **77** 045428
[90] Liu Z, Liu C-X, Wu Y-S, Duan W-H, Liu F and Wu J 2011 *Phys. Rev. Lett.* **107** 136805
[91] Wada M, Murakami S, Freimuth F and Bihlmayer G 2011 *Phys. Rev. B* **83** 121310
[92] Zhang H, Freimuth F, Bihlmayer G, Blügel S and Mokrousov Y 2012 *Phys. Rev. B* **86** 035104

[93] Huang Z-Q, Chuang F-C, Hsu C-H, Liu Y-T, Chang H-R, Lin H and Bansil A 2013 *Phys. Rev. B* **88** 165301

[94] Chen L, Wang Z F and Liu F 2013 *Phys. Rev. B* **87** 235420

[95] Hsu C-H, Ozolins V and Chuang F-C 2013 *Surf. Sci.* **616** 149

[96] Xu Y, Yan B, Zhang H-J, Wang J, Xu G, Tang P, Duan W and Zhang S-C 2013 *Phys. Rev. Lett.* **111** 136804

[97] Hsu C-H, Chang H-R, Chuang F-C, Liu Y-T, Huang Z-Q, Lin H, Ozolinš V and Bansil A 2014 *Surf. Sci.* **626** 68

[98] Zhou M, Ming W, Liu Z, Wang Yao Y and Liu F 2014 *Sci. Rep.* **4** 07102

[99] Zhou M, Ming W, Liu Z, Wang Z, Li P and Liu F 2014 *Proc. Natl. Acad. Sci. U.S.A.* **111** 14378

[100] Hsu C-H, Huang Z-Q, Chuang F-C, Kuo C-C, Liu Y-T, Lin H and Bansil A 2015 *New J. Phys.* **17** 025005

[101] Aktürk E, Aktürk O U and Ciraci S 2016 *Phys. Rev. B* **94** 014115

[102] Bieniek M, Woniak T and Potasz P 2017 *J. Phys.: Condens. Matter* **29** 155501

[103] Guo Y, Pan F, Ye M, Sun X, Wang Y, Li J, Zhang X, Zhang H, Pan Y, Song Z, Yang J and Lu J 2017 *ACS Appl. Mater. Interfaces* **9** 23128

[104] Kadioglu Y, Kilic S B, Demirci S, Aktürk O U, Aktürk E and Ciraci S 2017 *Phys. Rev. B* **96** 245424

[105] Zhang R, Zhang C-W, Ji W-X, Yan S and Yao Y 2017 *Nanoscale* **9** 8207 [Correction: *Nanoscale* 2017 **9** 11814]

[106] Wang X, Bian G, Xu C, Wang P, Hu H, Zhou W, Brown S A and Chiang T-C 2017 *Nanotechnology* **28** 395706

[107] Gao H, Wu W, Hu T, Stroppa A, Wang X, Wang B, Miao F and Ren W 2018 *Sci. Rep.* **8** 7346

[108] Lu Y, Xu W, Zeng M, Yao G, Shen L, Yang M, Luo Z, Pan F, Wu K, Das T, He P, Jiang J, Martin J, Feng Y P, Lin H and Wang X-s 2015 *Nano Lett.* **15** 80

[109] Munoz F, Vergniory M G, Rauch T, Henk J, Chulkov E V, Mertig I, Botti S, Marques M A L and Romero A H 2016 *Sci. Rep.* **6** 21790

[110] Wang Z F, Chen L and Liu F 2014 *Nano Lett.* **14** 2879

[111] Dil J H 2009 *J. Phys.: Condens. Matter* **21** 403001

[112] Chen Y L, Analytis J G, Chu J-H, Liu Z K, Mo S-K, Qi X L, Zhang H J, Lu D H, Dai X, Fang Z, Zhang S C, Fisher I R, Hussain Z and Shen Z-X 2009 *Science* **325** 178

[113] Park C-H and Louie S G 2012 *Phys. Rev. Lett.* **109** 097601

[114] Bian G, Zhang L, Liu Y, Miller T and Chiang T-C 2012 *Phys. Rev. Lett.* **108** 186403

[115] Wang Y H, Hsieh D, Pilon D, Fu L, Gardner D R, Lee Y S and Gedik N 2011 *Phys. Rev. Lett.* **107** 207602

[116] Bahramy M S, King P D C, de la Torre A, Chang J, Shi M, Patthey L, Balakrishnan G, Hofmann Ph, Arita R, Nagaosa N and Baumberger F 2012 *Nat. Commun.* **3** 1159

[117] Mirhosseini H and Henk J 2012 *Phys. Rev. Lett.* **109** 036803

[118] Scholz M R, Sánchez-Barriga J, Braun J, Marchenko D, Varykhalov A, Lindroos M, Wang Y J, Lin H, Bansil A, Minár J, Ebert H, Volykhov A, Yashina L V and Rader O 2013 *Phys. Rev. Lett.* **110** 216801

[119] Sánchez-Barriga J, Varykhalov A, Braun J, Xu S-Y, Alidoust N, Kornilov O, Minár J, Hummer K, Springholz G, Bauer G, Schumann R, Yashina L V, Ebert H, Hasan M Z and Rader O 2014 *Phys. Rev. X* **4** 011046

[120] Mirhosseini H, Maznichenko I V, Abdelouahed S, Ostanin S, Ernst A, Mertig I and Henk J 2010 *Phys. Rev. B* **81** 073406

[121] Braun J 1996 *Rep. Prog. Phys.* **59** 1267

[122] Braun J, Minár J and Ebert H 2018 *Phys. Rep.* **740** 1

[123] Braun J, Miyamoto K, Kimura A, Okuda T, Donath M, Ebert H and Minár J 2014 *New J. Phys.* **16** 015005

[124] Gray A X, Papp C, Ueda S, Balke B, Yamashita Y, Plucinski L, Minár J, Braun J, Ylvisaker

E R, Schneider C M, Pickett W E, Ebert H, Kobayashi K and Fadley C S 2011 *Nat. Mater.* **10** 759
[125] Minár J, Braun J and Ebert H 2013 *J. Electron. Spectrosc. Relat. Phenom.* **190** 159
[126] Hirahara T, Fukui N, Shirasawa T, Yamada M, Aitani M, Miyazaki H, Matsunami M, Kimura S, Takahashi T, Hasegawa S and Kobayashi K 2012 *Phys. Rev. Lett.* **109** 227401
[127] Hirahara T, Bihlmayer G, Sakamoto Y, Yamada M, Miyazaki H, Kimura S-i, Blügel S and Hasegawa S 2011 *Phys. Rev. Lett.* **107** 166801
[128] Yang F, Miao L, Wang Z F, Yao M-Y, Zhu F, Song Y R, Wang M-X, Xu J-P, Fedorov A V, Sun Z, Zhang G B, Liu C, Liu F, Qian D, Gao C L and Jia J-F 2012 *Phys. Rev. Lett.* **109** 016801
[129] Kim S H, Jin K-H, Park J, Kim J S, Jhi S-H, Kim T-H and Yeom H W 2014 *Phys. Rev. B* **89** 155436
[130] Miao L, Yao M Y, Ming W, Zhu F, Han C Q, Wang Z F, Guan D D, Gao C L, Liu C, Liu F, Qian D and Jia J-F 2015 *Phys. Rev. B* **91** 205414
[131] Yao M-Y, Zhu F, Han C Q, Guan D D, Liu C, Qian D and Jia J-f 2016 *Sci. Rep.* **6** 21326
[132] Klimovskikh I I, Sostina D, Petukhov A, Rybkin A G, Eremeev S V, Chulkov E V, Tereshchenko O E, Kokh K A and Shikin A M 2017 *Sci. Rep.* **7** 45797
[133] Wells J W, Dil J H, Meier F, Lobo-Checa J, Petrov V N, Osterwalder J, Ugeda M M, Fernandez-Torrente I, Pascual J I, Rienks E D L, Jensen M F and Hofmann Ph 2009 *Phys. Rev. Lett.* **102** 096802
[134] Drozdov I K, Alexandradinata A, Jeon S, Nadj-Perge S, Ji H, Cava R J, Bernevig B A and Yazdani A 2014 *Nat. Phys.* **10** 664
[135] Kawakami N, Lin C-L, Kawai M, Arafune R and Takagi N 2015 *Appl. Phys. Lett.* **107** 031602
[136] Yeom H W, Jin K-H and Jhi S-H 2016 *Phys. Rev. B* **93** 075435
[137] Fu L and Kane C L 2007 *Phys. Rev. B* **76** 045302
[138] Sabater C, Gosálbez-Martínez D, Fernández-Rossier J, Rodrigo J G, Untiedt C and Palacios J J 2013 *Phys. Rev. Lett.* **110** 176802
[139] Pumera M and Sofer Z 2017 *Adv. Mater.* **29** 1605299
[140] Reis F, Li G, Dudy L, Bauernfeind M, Glass S, Hanke W, Thomale R, Schäfer J and Claessen R 2017 *Science* **357** 287
[141] Nicolaï L, Minár J, Mariot J-M, Djukic U, Richter M-C, Heckmann O, Balasubramanian T, Leandersson M, Sadowski J, Braun J, Ebert H, Denlinger J, Vobornik I, Fujii J, Gmitra M and Hricovini K 2018 arXiv:1806.03061
[142] Fu L 2011 *Phys. Rev. Lett.* **106** 106802